Original Article

Monte Carlo study of MLC fields for cobalt therapy machine

Komanduri M. Ayyangar, Roopa A. Rani, Anil Kumar[1], A. R. Reddy

International Cancer Center, Mahatma Gandhi Memorial Medical Trust, Peda Amiram, Bhimavaram, Andhra Pradesh, [1]MNJ Institute of Oncology and Regional Cancer Center, Red Hills, Hyderabad, India

Submission on: 18.10.2013 Review completed on: 14.02.2014 Accepted on: 14.02.2014

ABSTRACT

An automated Multi-Leaf Collimator (MLC) system has been developed as add-on for the cobalt-60 teletherapy machines available in India. The goal of the present computational study is to validate the MLC design using Monte Carlo (MC) modeling. The study was based on the Kirloskar-supplied Phoenix model machines that closely match the Atomic Energy of Canada Limited (AECL) theratron-80 machine. The MLC is a retrofit attachment to the collimator assembly, with 14 non-divergent leaf pairs of 40 mm thick, 7 mm wide, and 150 mm long tungsten alloy plates with rounded edges and 20 mm tongue and 2 mm groove in each leaf. In the present work, the source and collimator geometry has been investigated in detail to arrive at a model that best represents the measured dosimetric data. The authors have studied in detail the proto-I MLC built for cobalt-60. The MLC field sizes were MC simulated for 2 × 2 cm^2 to 14 × 14 cm^2 square fields as well as irregular fields, and the percent depth dose (PDD) and profile data were compared with ROPS† treatment planning system (TPS). In addition, measured profiles using the IMATRIXX system‡ were also compared with the MC simulations. The proto-I MLC can define radiation fields up to 14 × 14 cm^2 within 3 mm accuracy. The maximum measured leakage through the leaf ends in closed condition was 3.4% and interleaf leakage observed was 7.3%. Good agreement between MC results, ROPS and IMATRIXX results has been observed. The investigation also supports the hypothesis that optical and radiation field coincidence exists for the square fields studied with the MLC. Plots of the percent depth dose (PDD) data and profile data for clinically significant irregular fields have also been presented. The MC model was also investigated to speed up the calculations to allow calculations of clinically relevant conformal beams.

†Radiation Oncology Planning System (ROPS) is supplied by Tirumala Jyothi Computer Systems described at https://sites.google.com/site/tjcsrops/

‡IMATRIXX is supplied by IBA Dosimetry described at HYPERLINK http://www. iba-dosimetry. com

Key words: BEAMnrc, Cobalt-60, MLC, Monte Carlo

Introduction

In a previous publication,[1] the Monte Carlo (MC) modeling of the cobalt machine using the approach published by Mora *et al.*,[2] in 1999 was presented. In that paper,[1] the cobalt source and the collimator systems were modeled using BEAMnrc software and showed that the central axis PDD matched with published values from British Journal of Radiology Supplement 25 (BJR25). The beam profiles for a 10 × 10 cm^2 field were presented; however, they were not compared with any realistic profile data. The model was used to test the MLC leakage using 6-cm tungsten leaves at a source distance of 48 cm. That paper[1] also presented the use of low melting point alloy (LMPA) and concluded that tungsten is preferable for the construction of the MLC leaves. The methodology of the current MC simulation follows the same approach as previously published.[1]

In AMPICON 2009 at Hyderabad, we presented a tungsten-based manual MLC that had 20 leaves that can cover a field size of 30 cm wide by 20 cm length.[3] The MLC was to be an add-on to existing therapy machine. Subsequently, proto-I MLC was successfully built and tested using a Phoenix model cobalt-60 teletherapy machine, with

Address for correspondence:
Dr. Komanduri M Ayyangar,
Mahatma Gandhi Memorial Medical Trust Hospital, Peda Amiram, Bhimavaram, Andhra Pradesh - 534 204, India.
Email: akomanduri@gmail.com

Access this article online	
Quick Response Code:	Website: www.jmp.org.in
	DOI: 10.4103/0971-6203.131279

80 cm isocenter distance, supplied by Kirloskar*. This MLC is a retrofit attachment to the collimator assembly, with 14 non-divergent leaf pairs of 40 mm thick, 7 mm wide, and 150 mm long tungsten alloy plates with 20 mm tongue and 2 mm groove in each leaf. The tongue and groove geometry of each leaf helps in minimizing the interleaf leakage of radiation especially when gaps are a possibility in the manufacture of the leaf. Some additional interleaf gap is essential for enabling smoother interleaf movement of the leaves. It was found that tongue and grove geometry also provides better holding of the leaves together. The 4 cm thick 14-leaf pair MLC was mounted as a sliding insert to the collimator with the bottom of the leaves at 56 cm from the bottom of the source. The proto-I MLC, a fully functional automated MLC fitted to Phoenix telecobalt machine, is shown in Figure 1. Details of leaf cross-section, leaf projection, leaf position accuracy, and leaf end transmission when MLC is fully closed, mid-leaf transmission, radiation output factors, PDDs as well as profiles for different square fields, triangular field and some clinical fields of this proto-I were presented in AMPICON 2010, 2011 and 2012.[4-7]

The leaves had rounded edges in the width direction and non-focused (parallel) in the length dimension. The dimensions of the leaves were 7 mm thick, 4 cm height, and 15 cm long. The curved end of each of the leaf had a radius of curvature of 4.25 cm and its extent from the chord was restricted to 5 mm to minimize the penumbra due to rounded end. The 7 mm leaf width projected a leaf width of 10 mm at the isocenter. The centers of the rounded edges were at 54 cm from the source, and they define the optical field as well as radiation field. The MLC mount had a locking mechanism to fix the MLC centered on the central axis of the radiation beam.

It is assumed that the cobalt source of the Phoenix machine is in the form of radioactive cobalt pellets encapsulated in a 1.5 cm diameter and 2 cm height steel cladding. The exact dimensions and materials of the source and the pellet packing density were not available.

The simulated machine dimensions mentioned in the previous publication,[1] although given good agreement with PDD data, the profile data were not satisfactory at all field sizes. With the current MC investigation, it was quickly learned that while the opening at the lower end of the collimator defined the field size, the upper end of the collimator has to ensure no part of the source is masked. If the opening of the upper end of the collimator is too wide, it affects the PDD and profiles. This fact has been already mentioned by Mora *et al*.,[2] in their publication.

Sahani *et al*.,[8] have extensively studied an MLC design for cobalt machine. Although there are many similarities, to the current investigation, there are some notable differences. Their MLC design was for a source to MLC distance of 38 cm and requires a replacement of the current collimation system for existing cobalt machines. Their MLC defines the primary beam aperture, instead of the telescopic collimator that exists in the cobalt therapy machines. In addition, their MLC leaves were 7 cm thick, whereas in the current study they were 4 cm thick. Our current MC simulation computational study is for an actually fabricated retrofit system. As mentioned above some physical and radiation characteristics of this system were previously reported.[4-7] Singh *et al*.,[9] have also reported a motorized MLC for cobalt-60; however, the project was later discontinued.

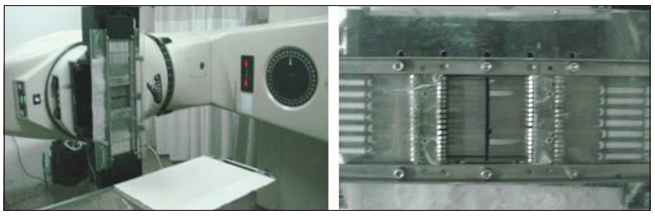

Figure 1: First prototype of the automated fully functional MLC fitted to telecobalt machine with MLC leaves shown in the fully closed position

The aim of the present study was to generate the PDD as well as beam profiles for various square and irregular MLC fields simulated with MC. These data were already compared with experimentally measured data using the proto-I MLC and satisfactory agreement was obtained. These studies were presented[4-7] and a separate paper is in the process of preparation. However, some limited experimental measurements using the IMATRIXX were also compared with the MC profiles in this paper. The ROPS treatment planning system (TPS) has been previously validated[7] using BJR25-published PDD tables and a set of beam profiles obtained from a generic AECL cobalt-60 beam data. Because MLC for cobalt was not previously available, the ROPS TPS is now being validated using the MC data from this study. The ROPS dose calculation algorithm for MLC fields is based on Clarkson scatter summation of the open portion of the leaves. In addition it uses a measured fluence factor table based on MLC field configurations.

One of the goals of this investigation was to study the optical field and radiation field congruence.

In addition, our aim of the study was also to modify the simulation geometry to speed up the MC simulations.

Materials and Methods

MC simulation

Each simulation requires defining the parameters in an independent input file. The photons that reach the isocenter were captured in a file called "phase space file".

*Kirloskar Technologies (P) Ltd., B-58, Defence Colony, 1st floor, Bhishma Pitamah Marg, New Delhi - 110 024, India.

This file scores the position, direction, and energy of the photons. In addition, using the latch parameter, one can track the origin of the photon. In this investigation, the latch parameter was not set. Three open square fields of sizes 5 × 5, 10 × 10 and 15 × 15 cm^2 were simulated in three independent simulations. Typically, each simulation had 2-3 billion histories and took 45 h on the Pentium Intel Core i5 2.53 GHz, 4 Gb random access memory (RAM) laptop, in the high performance mode. It was observed that unless the high performance mode is selected on the laptop, the simulations took twice as much time. After the simulation, dose was calculated for a 30 × 30 × 25 cm^3 phantom using DOSXYZnrc program. The matrix size chosen for this step was 5 × 5 × 5 voxels. Decreasing the voxel size to 2.5 × 2.5 × 2.5 mm^3 increased the computation time while there was no significant benefit [see Appendix A]. These voxels were centered at each dose matrix point of interest, i.e. 2.5 mm around the point of calculation. The voxels in the x and y directions span a range of −15.25 cm to +15.25 cm using 61 voxels in each direction. The z direction that corresponds with the beam depth had 51 voxels with the first voxel defined from 0-2.5 mm and 50 voxels covering 0.25-25.25 cm depth. Thus, the second voxel is centered on dmax for cobalt beam. The phantom size was reduced for smaller field sizes. The standard deviation of dose calculated using 10 batches was typically less than 1%. Separate programs have been developed to read the DOSXYZnrc output file and extract planar data or PDD or profile data that can be exported to Microsoft EXCEL software for generating graphical data.

The MLC leaves were fabricated through powder metallurgy route using a tungsten alloy (94.5% W, 2.5% Ni, 1.8% Fe, Cu, Co, and 0.6% Ta) and had a density of 17.75 g cm^{-3}. For the MC simulation, an alloy of tungsten was used as supplied in the electron gamma shower (EGS) distribution in pegs4/data with 95% W, 1.5% Cu, and 3.5% Ni with a density of 18 g cm^{-3}, which matched closely with the alloy used to fabricate the leaves.

The criteria for good agreement between simulation and either calculation or measurement is taken as less than 2 mm difference in full width at half maximum (FWHM) and less than 2% agreement with central axis PDD for all field sizes.

Source-collimator configuration

Two source-collimator configurations were used: First, the full cobalt machine configuration with all the components of the telescopic collimator; second, a virtual cobalt configuration that was adjusted to match the expected results at the same time to provide fast simulation. These configurations are depicted in Figure 2.

The cobalt source was assumed to be a solid cobalt source cylinder of diameter 1.5 cm and height 2.0 cm. When source cladding was used, the source was surrounded by a 1 mm steel sheet. In the first configuration, as shown in Figure 2a the source with cladding, the primary collimator with fixed opening, and the telescopic collimator with four sections were simulated. The telescopic collimator follows the beam divergence defined by the periphery of the source bottom as defined by Mora *et al*.,[2] and Sahani *et al*.,[8]

In the virtual source configuration, as shown in Figure 2b the source cladding and the primary collimator were not simulated as they had an imperceptible effect on the clinically used beam. In addition, the four sections of the telescopic collimator were coalesced into one section with 15 cm effective lead thickness. In this configuration, the beam divergence follows the periphery of the source top. The lines from the edges of the source to the upper end of the jaws dictate the opening needed at the upper end. The lines that follow from the bottom of source center to the isocenter dictate the beam dimension at the isocenter. Because the optical field is defined from a point source situated at the bottom center of the cobalt source, the lower end of the collimator defines the optical field. The radiation field width is modified by the transmission penumbra and can be determined only after the MC simulation. More details for clarity on source size, light source position, and their relationship and impact on focal point of telescopic collimator and penumbra factor as well as on geometric and radiation-defined FWHM are given in Appendix B.

Experimental measurements using IMATRIXX

For comparison of MC data with experiment, one needs accurate PDD and profile data. Using point measurements in water, it has been previously proved that BJR25 tables of cobalt-60 PDD for 80 cm source to skin distance (SSD) closely match the current therapy machine. Unfortunately, due to inadequate clearance of the machine, water scanner measurements were not possible, instead the IMATRIXX system with virtual water was used. While comparing Cobalt-60 PDD, it was observed that 10 cm of virtual water is equivalent to 10.24 cm of real water. However, the profile measurements were expected to be close. The IMATRIXX is an array of ion chambers embedded in a flat plastic phantom. It was made by SUN Nuclear and marketed by IBA Dosimetry as ImRT MAtriXX. The effective point of measurement for each detector was 3 mm from surface. By adding 2 mm virtual water, the measurement depth was set to dmax. Additional virtual water slabs were added for other required depths. The 80 cm SSD was maintained on top of the 2 mm virtual water slab. The IMATRIXX gave the complete planar data as an American Standard Code for Information Interchange (ASCII) file. The IMATRIXX detectors come prearranged in a 32 × 32 matrix separated by 7.62 mm. The ion chambers were cylindrical with 4.5 mm diameter by 5 mm height. There was no detector at the central axis position. There were four detectors 5.4 mm away in the four corners from the central axis.

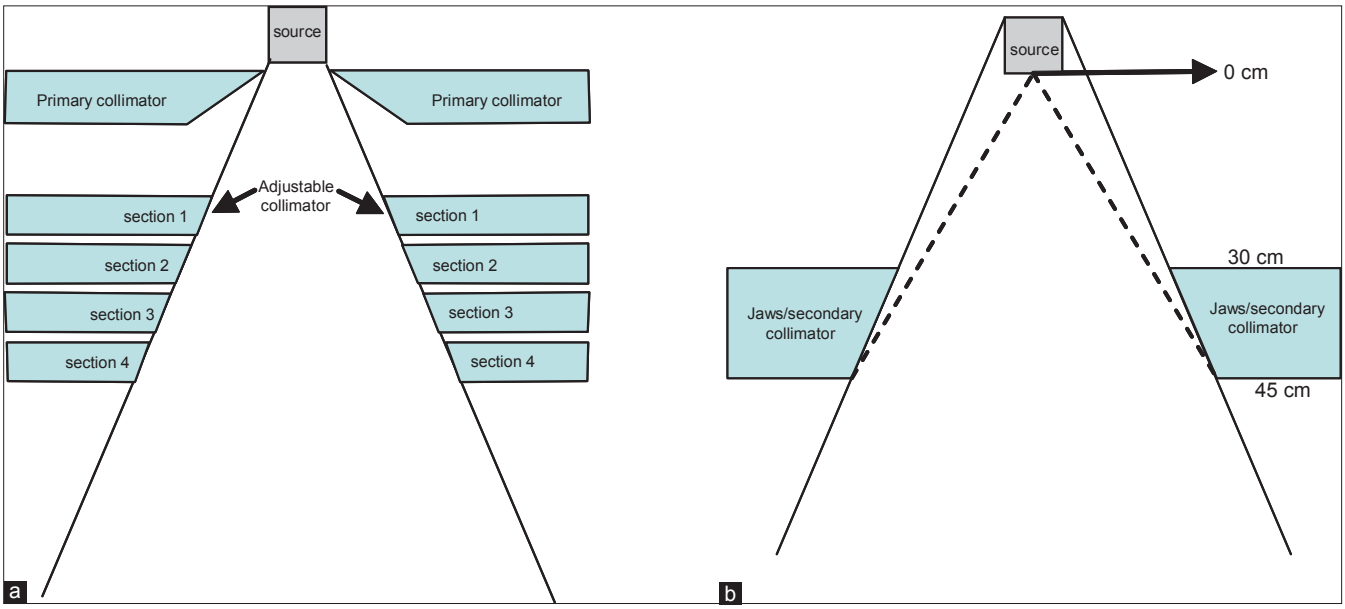

Figure 2: Source and collimator geometry of the (a) Full cobalt machine and the (b) Virtual machine. (Not drawn to scale)

In view of the detector to detector distance and detector size, one can expect positional inaccuracies up to 3.8 mm. In addition, data could show the effect of smearing due to chamber size. The MLC was used with IMATRIXX to collect data with square fields of 2 × 2 to 10 × 10 cm^2 and rectangular fields for 2 × 14 to 10 × 14 cm^2 at 2-cm intervals with jaws set at 14 × 14 cm^2 at 80 cm SSD for 5 cm depth.

Square field simulation

As mentioned earlier, three fields of size 5 × 5, 10 × 10, and 15 × 15 cm^2 were chosen for square field simulations. The simulations were conducted independently, as there is no facility in BEAMnrc to define multiple simulations in one input file. The primary collimator, made of lead, has a fixed opening to cover all the fields sizes 2 × 2 to 35 × 35 cm^2. The telescopic collimator has four sections as shown in the Figure 2. The outer collimator was mounted at 45 cm. The MLC component was used only when MLC fields were simulated. The phase space file was scored at a distance of 80 cm from the source in a rectangualar area of 25 × 25 cm^2 defined perpendicualr to the beam central axis. The empty space was filled with air. It is important to define air, if not electron contamination would increase surface dose.

One of the goals of the present study was to investigate on how to speed up the MC computations. One of the reasons for the increase in computation time is the complex arrangement of the telescopic collimator and the source configuration. To speed up the MC calculation process, the source cladding and the primary collimator were removed. In addition, instead of using multi-section telescopic secondary collimator, the four sections of the telescopic collimator were coalesced into a single rectangular collimator. Further, this secondary collimator was of 15 cm height starting at 30 cm from source and ending at 45 cm. By trial and error, the radiation properties of this virtual machine were ensured to be equivalent to the full machine simulation. Except for the square field simulation, which was done with full machine simulation, all the rest of the simulations in this study were done with the virtual machine simulation. All simulations typically were calculated with 2 billion histories and resulted in nearly 1% standard deviation at 10 cm depth.

Results and Discussion

Square field simulation

As mentioned before, the BEAMnrc simulation was done for 2-3 billion histories. The DOSXYZnrc program will only use the particles from the phase space file and can reuse the particles if more histories than existing in the phase space file were requested. The DOSXYZnrc simulation was done by recycling the photons in phase space file by a factor of 100. In addition, a photon splitting number 10 was used. Even though DOSXYZnrc reuses the photons, each photon's travel inside the phantom was followed by EGS code using MC methods. Typical data from the full machine geometry simulations are tabulated in Table 1. It can be seen that it took about 50-70 h of computation to achieve 0.9% standard deviation.

Comparison of PDD values from MC Simulations and ROPS

Table 2 shows the comparison of PDD calculated from MC simulations of square fields and those obtained from the BJR25 data and ROPS-calculated data. It can be seen that the agreement in all the cases of simulation of telecobalt machine and the virtual machine with BJR25 and ROPS data is good and is within 2%. In an earlier study,[7] it has been demonstrated that ROPS PDD agrees with BJR25 within 1%. The ROPS

planning system was used with the dose calculation mode set to Clarkson-type scatter integration method.

Comparison of profile data between MC computations and ROPS

Table 3 shows profile data comparison with geometrically expected FWHM for all the three field sizes. It can be seen that the deviations are less than 2 mm and would satisfy the safety requirements.

The results of PDD and FWHM, as shown in Tables 2-3 closely matched with those of the full machine simulation as well as ROPS. Once again the agreement can be seen to be acceptable.

Figure 3 shows a comparison of MC data for open fields with ROPS and IMATRIXX for the field sizes of 4 × 4, 5 × 5, 10 × 10 and 15 × 15 for various depths. It can be seen that the agreement is reasonable.

This establishes that the MC simulation correctly models the cobalt-60 teletherapy machine.

Figure 4 shows the profile comparison of the 10 × 10 cm^2 field of the virtual machine computed using 2-3 billion histories with those calculated using ROPS as representative profiles for both x and y-directions at depths dmax and at 20 cm. This established the use of the virtual machine simulation in MC computations.

Table 1: BEAMnrc and DOSXYZ simulation of square fields

Field size (cm^2)	*Number of histories ($\times 10^9$)*	*Number of photons in phase space file ($\times 10^6$)*	*Standard deviation at 10 cm depth on central axis (%)*	*BEAMnrc computation time (h)*	*DOSXYZnrc computation time (h)*
5×5	3.0	1.02	0.9	50	7
10×10	2.5	3.14	0.9	42	12
15×15	2.0	5.55	0.9	45	24

Table 2: Comparison of PDD of MC-simulated square fields with BJR25 and ROPS data

Field size (cm^2)	*Depth (cm)*	*ROPS PDD*	*BJR25 PDD*	*Full machine PDD*	*Percent difference with MC*		*Virtual machine PDD*	*Percent difference with MC*	
				MC	*BJR25*	*ROPS*	*MC*	*BJR25*	*ROPS*
5×5	5	74.7	75.2	75.7	0.7	1.3	75.9	0.9	1.6
	10	51.6	51.2	51.5	0.6	−0.2	51.8	1.2	0.4
	20	23.2	23.2	23.2	0.2	0.2	23.3	0.2	0.4
10×10	5	78.4	78.8	78.5	−0.4	0.1	78.5	−0.4	0.1
	10	55.7	56.4	56.3	−0.2	1.0	55.9	−0.8	0.4
	20	27.3	27.4	27.1	−1.0	−0.7	27.7	1.2	1.1
15×15	5	79.9	80.3	79.7	−0.8	−0.3	80.8	0.7	1.1
	10	58.5	59.2	58.8	−0.7	0.5	58.2	−1.7	−0.5
	20	30.3	30.2	29.7	1. 7	2.0	30.6	1.3	1.0

MC: Monte carlo, PDD: Percent depth dose

Table 3: Comparison of expected and observed FWHM of profile data for both x- and y- directions from MC computations

Field size (cm×cm)	*Depth (cm)*	*Profile direction*	*FWHM expected (cm)*	*Full machine simulation*		*Virtual machine simulation*	
				FWHM observed (cm)	*Difference (mm)*	*FWHM observed (cm)*	*Difference (mm)*
5×5	0.5	x	5	5.19	1.9	5.08	0.8
	0.5	y	5	5.18	1.8	5.09	0.9
	20	x	6.25	6.5	2.5	6.43	1.8
	20	y	6.25	6.48	2.3	6.45	2.0
10×10	0.5	x	10	10.16	1.6	10.1	1.0
	0.5	y	10	10.14	1.4	10.17	1.7
	20	x	12.5	12.64	1.4	12.6	1.0
	20	y	12.5	12.62	1.2	12.55	0.5
15×15	0.5	x	15	15.13	1.3	15.05	0.5
	0.5	y	15	15.2	2.0	15.07	0.7
	20	x	18.75	18.91	1.6	18.84	0.9
	20	y	18.75	18.9	2.5	18.7	−0.5

MC: Monte carlo

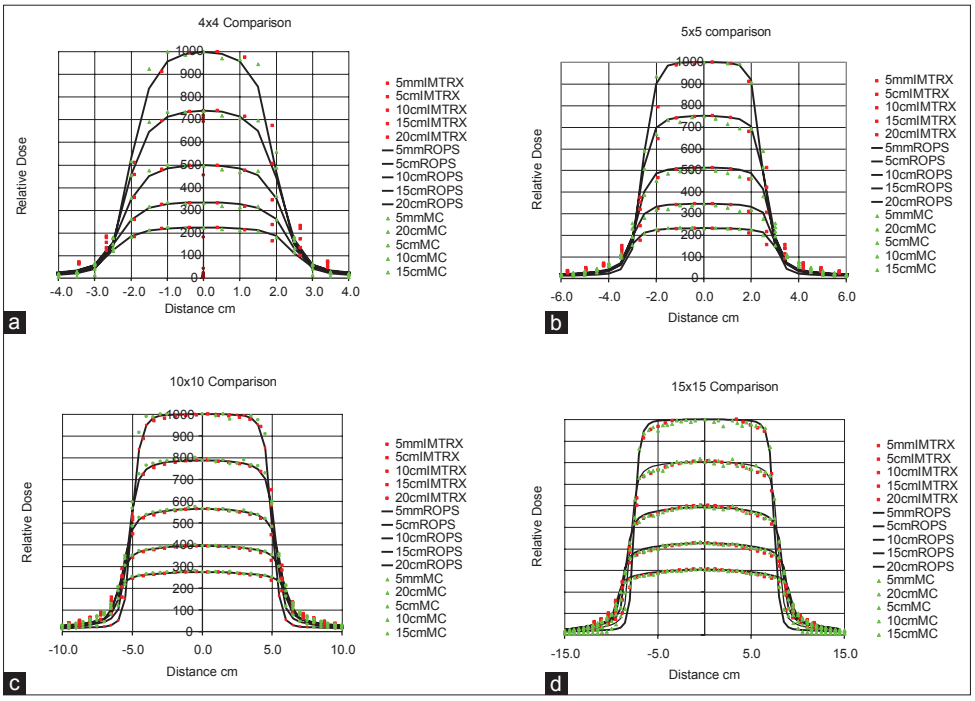

Figure 3: Comparison of MC with ROPS and IMATRIXX for 4 × 4, 5 × 5, 10 × 10, and 15 × 15 fields. ROPS data are shown as continuous lines. The MC data are shown in green triangles and IMATRIXX data in red squares. MC = Monte Carlo

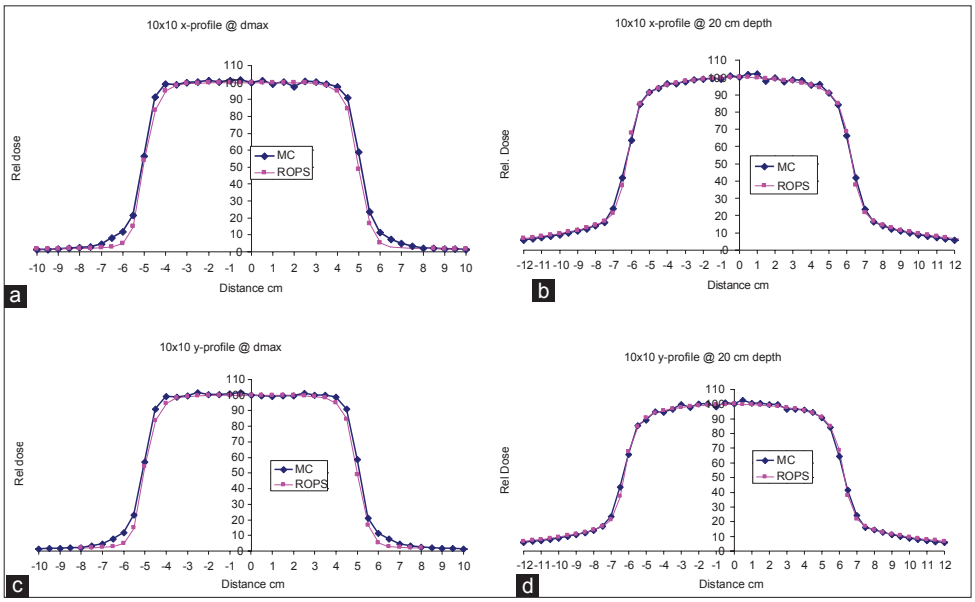

Figure 4: Comparison of profiles generated from computations with virtual machine MC simulation and with ROPS. (a) The x-profile comparison of MC with ROPS for 10 × 10 cm² field for depths dmax and 20 cm. (b) The y-profile comparison of MC with ROPS for 10 × 10 cm² field for depths dmax and 20 cm. MC = Monte Carlo

Although the profiles matched within 2 mm compared with expected values, some data shown above have exceeded this limit. This has been investigated extensively using MC simulations of various source geometry configurations and some results were given in the Appendix B. There is a definite uncertainty in the exact source dimensions and materials that match the cobalt source. Similarly, carefully measured accurate experimental data were not available. When such data become available, it would be possible to model the cobalt machine to get better agreement with measured data.

MLC square field simulation

The configuration of the 28 leaf proto-I MLC for telecobalt machines has been described earlier. Using the BEAMnrc MC technique, various square fields set by the MLC have been simulated using the virtual machine configuration. Except for the fields 2 × 2 and 4 × 4 cm², the jaws of the secondary

collimator were always set just to cover the outer boundary of the MLC field. For 2 × 2 cm² field, the jaws could not be closed below 4.5 × 4.5 cm. The results of PDD and profiles were compared with ROPS TPS data. The x-direction was defined as parallel (cross plane) to the MLC leaves and the y-direction was perpendicular (in-plane) to the leaves.

The computation time for 2 billion histories for the virtual source using BEAMnrc was in the range of 5-6 h, whereas the DOSXYZ program took 5-6 h. This results in a standard deviation of about 1%.

Scatter plots

Figure 5 depicts the scatter plot of the photons in the phase space file for the 2 × 2 cm² MLC field. This represents the incident fluence on the phantom. Notice the interleaf leakage in the y-direction. Leakage was also seen for triangle and brain fields, the results of which are presented later in this paper.

Scatter plots for a 6 × 6 cm² are shown in Figure 6a with jaws just covering the 6 × 6 cm² field and Figure 6b for the same 6 × 6 cm² field with jaws open up to 20 × 14 cm² field. In Figure 6a, there is practically no radiation beyond the 6 × 6 cm² area. However, there will be small amount of scatter and transmission of radiation through blocked primary jaws and MLC leaves. In Figure 6b, we see the complete properties of the MLC. Here, the jaws play no role, as they were open to 20 × 14 cm² size. First of all there was the 6 × 6 cm² region seen as dark area. Next there was interleaf leakage of nearly 20% in the y-direction close to central in-plane. This is where the rounded ends meet. Lastly, there was nearly 3% transmission leakage (it was 3.4% by measurement) all across the 20 × 14 cm² field due to transmission of the 4 cm tungsten.

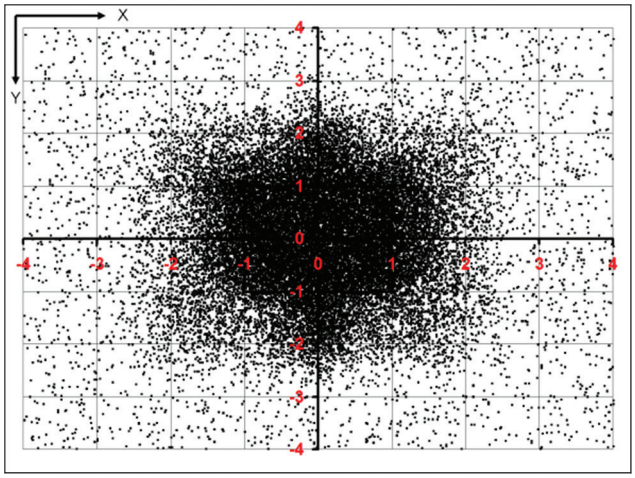

Figure 5: Scatter plot of the photons in the phase space file for the 2 × 2 cm² MLC field. The secondary collimator jaws were at 4.5 × 4.5 cm. Notice the interleaf leakage in the y-direction

Percent depth dose

Table 4 shows the PDD comparison of MC-simulated MLC fields 2 × 2 to 14 × 14 cm² with BJR25 PDD data.

It can be seen that the PDD agreement is mostly less than 4%. Some part of the disagreement is expected, as the BJR data are for open fields, whereas the MC data are for MLC fields. Scatter from the MLC would have an effect on the depth dose data. Figure 7 shows the PDD comparison of the MLC fields with ROPS planning system for a 10 × 10 cm² field. Similar PDD comparison for all other fields listed in Table 4 was made and good agreement was observed.

Profile data from MLC-defined fields

Table 5 shows profile data in terms of FWHM in x and y-directions for depths 0.5 cm and 20 cm for MLC-defined fields along with geometrically expected FWHM based on open field data. The collimator jaws for these were set to match the MLC open field size. It can be seen that the deviations are usually less than 1 mm except for the 2 × 2 cm² field. It is expected that the relative contribution of leakage and transmission is higher for small fields and hence the larger difference.

For all the MLC fields 2 × 2 to 14 × 14 cm², the x- and y-profiles at dmax and d = 20 cm were obtained from MC simulations and computations. Figure 8a and b shows comparison of MLC x and y-profiles at dmax obtained by MC and by ROPS for a representative 10 × 10 cm² field defined with the MLC. It can be seen from the results presented in

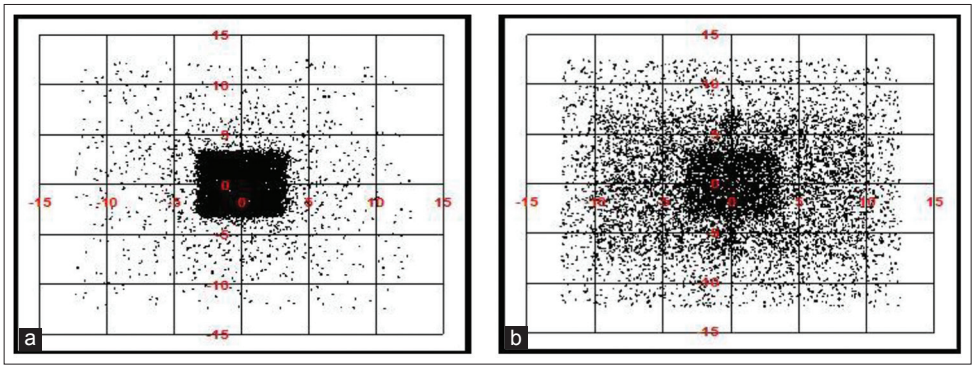

Figure 6: Scatter plots of 6 × 6 cm² simulation. (a) Jaws set at 6 × 6 cm² and (b) Jaws set at 20 × 14 cm². Notice the interleaf leakage and transmission leakage in (b)

Table 4: PDD comparison of MC-defined MLC fields with BJR25

Field size (cm×cm)	*Depth (cm)*	*BJR25*	*MC*	*Percent difference*
2×2	5	70.3	71.7	2.0
	10	46.3	46.9	1.4
	20	21.2	20.5	−3.5
4×4	5	73.9	74.4	0.7
	10	49.7	50.3	1.2
	20	22.2	22.7	2.4
6×6	5	76.2	76.3	0.1
	10	52.5	52.7	0.3
	20	24.1	24.1	0.2
8×8	5	77.8	80.2	3.1
	10	54.8	55.8	1.8
	20	25.8	25.6	−1.0
10×10	5	78.8	78.4	−0.5
	10	56.4	54.5	−3.4
	20	27.4	26.4	−3.7
12×12	5	79.5	82.4	3.6
	10	57.7	59.4	3.0
	20	28.7	28.7	−0.2
14×14	5	80	79.3	−0.9
	10	58.7	57.9	−1.3
	20	29.7	30.4	2.2

MC: Monte carlo, PDD: Percent depth dose

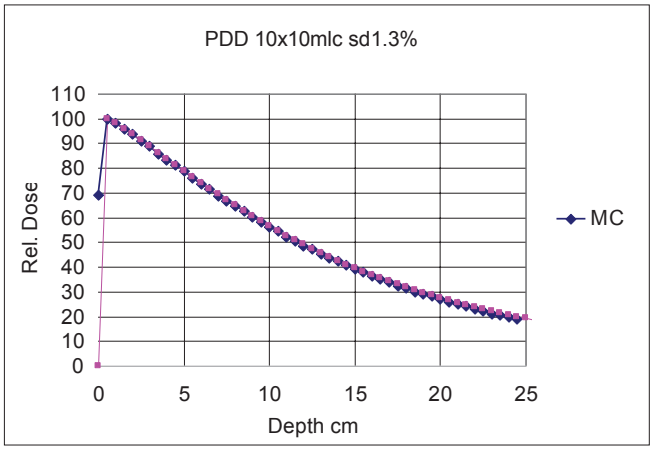

Figure 7: PDD comparison of 10 × 10 cm² square field defined by the MLC. The PDD comparison was made between MC simulation and ROPS treatment planning data. MC = Monte Carlo, PDD = percent depth dose

Table 5 and from the profiles that in general there is good agreement between MC and ROPS results. This also assures that optical and radiation field congruence exists for all the studied fields within acceptable safe limit of 1-2 mm.

Effect of collimator jaws on MLC

Because our MLC was designed with non-divergent leaves, normally the collimator jaws were set to block the MLC leaves except the open MLC area. To study the effect of collimator jaw settings, the MC simulations were done for the proto-1 MLC fields with the x-jaws fixed at 20 cm wide in the x-direction fully exposing the whole MLC with rounded leaves. The y jaws were fixed at 14-cm length, as our MLC cannot be used for more than 14 cm; otherwise radiation beam is not blocked beyond 14 cm. This test ensures the study of interleaf leakage and transmission leakage.

Table 5: Profile data from MLC-defined fields

Field size (cm×cm)	*Depth (cm)*	*Profile direction*	*FWHM expected*	*FWHM observed*	*Difference (mm)*
2×2	0.5	x	2	2.23	2.3
	0.5	y	2	2.28	2.8
	20	x	2.5	2.8	3.0
	20	y	2.5	2.77	2.7
4×4	0.5	x	4	4.01	0.1
	20	x	5	5.04	0.4
	0.5	y	4	4.01	0.1
	20	y	5	5.03	0.3
6×6	0.5	x	6	6.06	0.6
	0.5	y	6	6.06	0.6
	20	x	7.5	7.59	0.9
	20	y	7.5	7.55	0.5
8×8	0.5	x	8	8.1	1.0
	0.5	y	8	8.04	0.4
	20	x	10	10.06	0.6
	20	y	10	10.1	1.0
10×10	0.5	x	10	9.95	−0.5
	0.5	y	10	10.07	0.7
	20	x	12.5	12.52	0.2
	20	y	12.5	12.57	0.7
12×12	0.5	x	12	12.07	0.7
	0.5	y	12	12.13	1.3
	20	x	15	15.05	0.5
	20	y	15	15.05	0.5
14×14	0.5	x	14	13.94	−0.6
	0.5	y	14	14.04	0.4
	20	x	17.5	17.3	−2.0
	20	y	17.5	17.4	−1.0

MLC: Multi-leaf collimator, FWHM: Full width at half maximum

The Figure 8 c–f shows the x and y-profiles at dmax and at depth 20 cm for 10 × 10 cm². The brown-colored data are for the MLC with jaws covering the MLC borders, e.g. for 6 × 6 cm² MLC field, the jaws were set to 6 × 6 cm². The blue-colored data are with jaws fully open to 20 cm wide by 14 cm length. The FWHM for y-direction plots with open jaws is wider by 2-4 mm for all fields compared with jaws covering the MLC. This is mainly due to the interleaf leakage of the MLC leaves. In addition, the non-divergent leaves showed increase in FWHM, which could be observed off axis where interleaf leakage was absent. As expected, the 14 × 14 cm² field data did not show any difference even for the y-direction, as all leaves were fully open. There is good agreement between MC with jaws open and jaws covering MLC in all the x-direction plots especially at dmax. This indicates that our rounded leaves are as good as jaws and there is radiation and light field agreement to the same extent as can be expected by primary jaws.

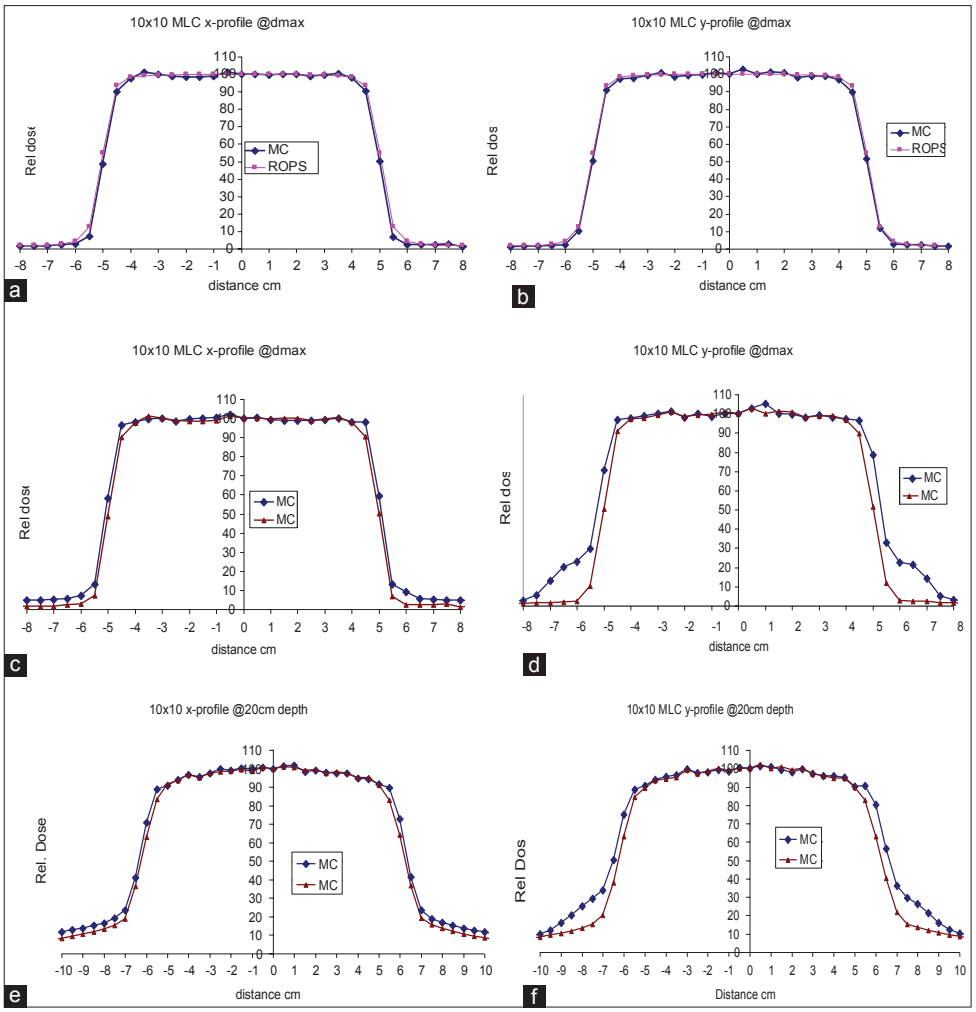

Figure 8: (a) Comparison of x-profiles generated by MC simulation with ROPS for 10 × 10 cm² field defined by the MLC at dmax. (b) Comparison of y-profiles generated by MC simulation with ROPS for 10 × 10 cm² field defined by the MLC at dmax. (c) Comparison of x-profiles at depth dmax generated by MC simulation of MLC 10 × 10 cm² field when two jaw settings were used. The brown-colored data are for the simulation with jaws set at 10 × 10 cm². The blue-colored data were with jaws set at 20 × 14 cm². (d) Similar comparison for y-profiles at dmax. (e) Similar comparison for x-profiles at 20 cm depth (f) Similar comparison for y-profiles at 20 cm depth. Notice the interleaf leakage in the penumbra area for the y-profiles when the jaws were opened beyond the MLC field. MC = Monte Carlo

The factors that influence the radiation field width have been extensively studied by Sahani *et al*. It was concluded that for better radiation field width and optical field congruence the distance between the source and the bottom of the MLC leaf should be larger; the height of the multileaf collimator leaf should be smaller and it is essential that a secondary collimator or its equivalence should be available. Our proto-1 MLC is an add-on to the telecobalt therapy machine and takes advantage of the existing secondary collimator already in the machine. The MLC of ours is (a) at larger distance from the source, 56 cm in ours versus 45 cm in Sahani *et al*.,'s study; (b) smaller in height, 4 cm in our case versus 7 cm in case of Sahani *et al*.; and (c) takes advantage of the existing secondary collimator to cover the non-required radiation field. Hence, we did not see problems in optical and radiation field agreement. They agree mostly within 2 mm for fields above 5 × 5 cm² as seen from the MC results in Table 5 even with the present non-divergent straight edge MLC leafs with 5-mm rounded end. Our rounded leaves are as good as jaws and there is radiation and light field agreement to the same extent as can be expected by primary jaws. In view of the above, our proto-1 MLC could be useful for conformal therapy.

MLC-defined irregular field simulation

Triangle-shaped field

To simulate the irregular field shapes, first a triangle-shaped beam was simulated. This triangle was chosen to assure asymmetry in left to right as well as top to bottom directions. This shape helps in ensuring the proper registration of the coordinate systems of ROPS and MC. The results of the MC simulation and comparison with those from ROPS are presented in Figure 9.

Figure 9 (a) shows a scatter plot of the triangle field

obtained from the MC simulation. Also shown is the outline of the triangle field. Notice the asymmetric shape of the field left to right and top to bottom. Figure 9b shows the MC versus ROPS comparison of the profiles for the triangle field in x and y-directions at dmax and 20 cm depths. Figure 9c shows the PDD comparison through central axis between MC and ROPS for the triangle field. Once again it can be seen that there is good agreement between them.

To test the irregular field simulation for clinically acceptable fields, three fields were chosen from a 3D conformal brain target plan. The plan used an anterior and two lateral beams with wedges to generate a 95% dose conforming plan. The fields were later used in the ROPS TPS to generate dose distributions in a 30 × 30 × 30 cm water equivalent phantom with the beams normally incident. No wedges were used for the simulated beams. These beams were defined in the MC simulations and the PDD as well as profiles were compared with ROPS data. Typical results obtained for one field are shown in Figure 10. The phantom sizes in MC and ROPS although are different to a small extent but both provide adequate scatter conditions. This clinical field was also measured with IMATRIXX and the comparison of MC with ROPS and IMATRIXX is shown in Figure 11.

Conclusions

The present investigation has demonstrated that the virtual cobalt machine simulated is adequate to match the PDD profiles of 80 cm isocenter cobalt machines available worldwide. The MLC proto-I that was designed and built and has been simulated on the virtual cobalt machine. The MLC field sizes were MC simulated for 2 × 2 cm^2 to 14 × 14 cm^2 square fields as well as irregular fields. The PDD and profile data obtained from MC computations were compared with ROPS TPS, which was previously commissioned using measured cobalt machine data. Generally good agreements between MC results and ROPS results have been observed. The investigation also supports the hypothesis that optical

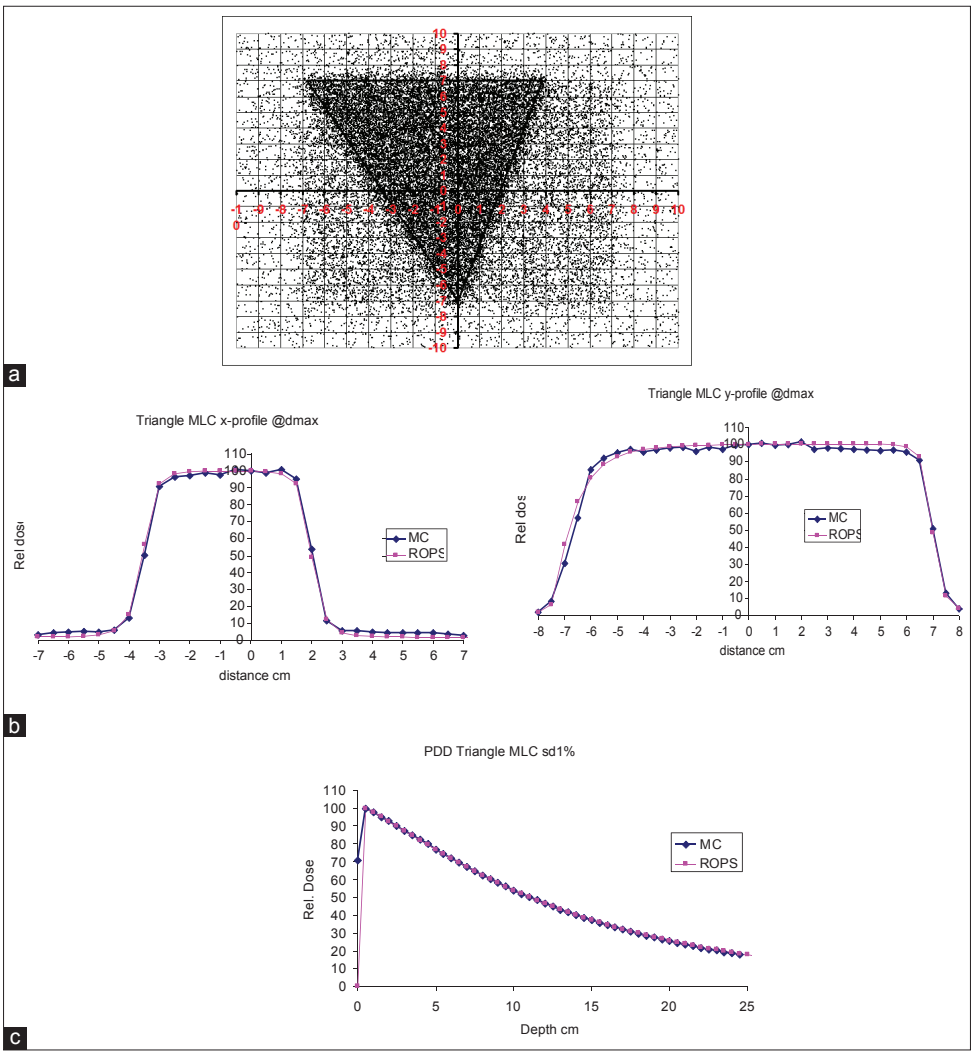

Figure 9: These figures show the MC versus ROPS comparison of the triangle field. (a) Scatter plot (b) profiles in x and y-directions at depth of dmax. (c) PDD plot comparison between MC and ROPS through the central axis of the triangle field. MC = Monte Carlo, PDD = percent depth dose

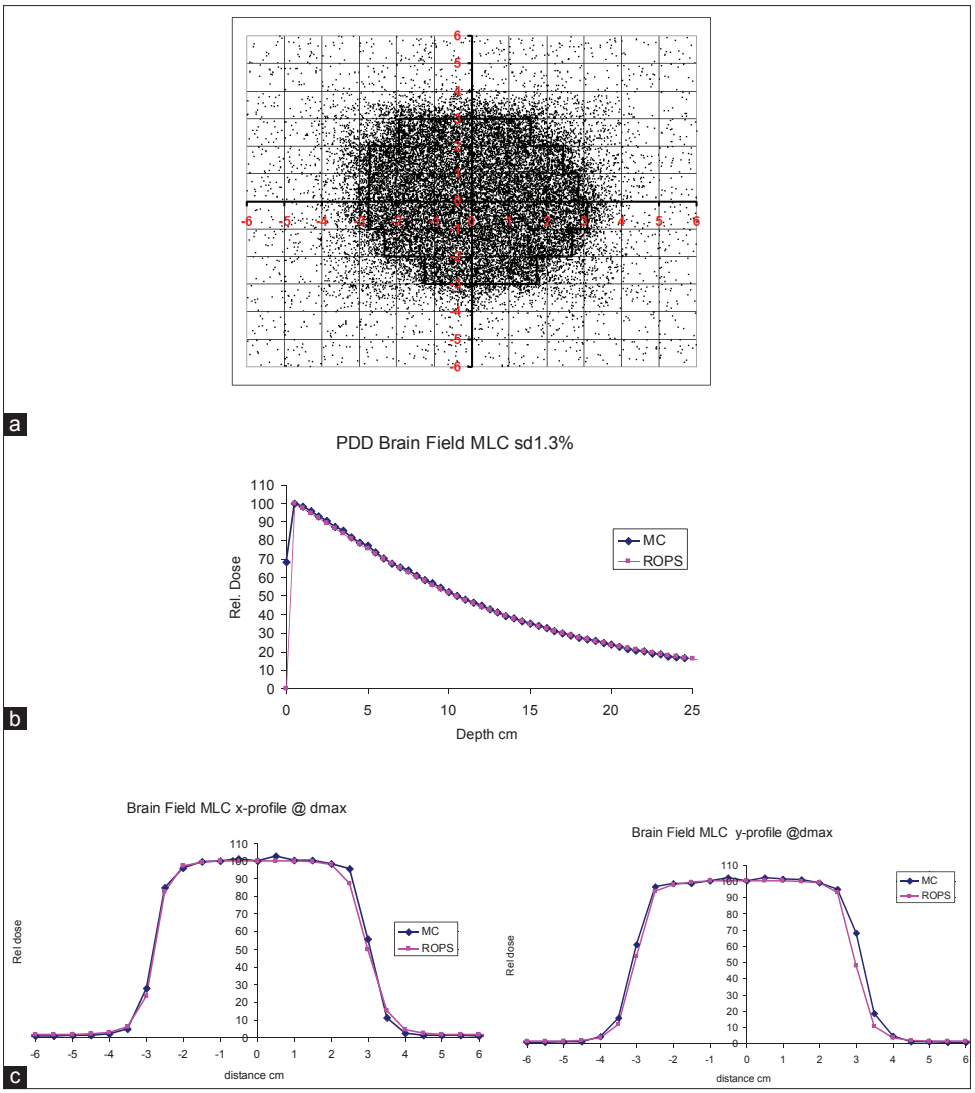

Figure 10: These figures show the MC versus ROPS comparison of the brain field 1. (a) Scatter plot and (b) PDD plot comparison between MC and ROPS through the central axis of the field. (c) Profile comparison in x and y-directions at dmax. MC = Monte Carlo, PDD = percent depth dose

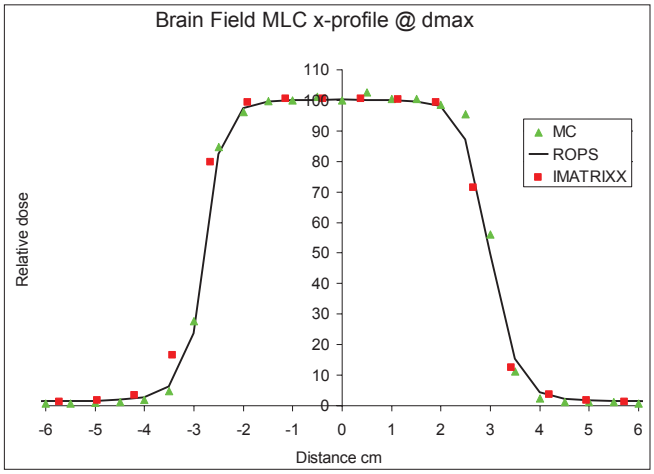

Figure 11: Comparison of MC data with ROPS and IMATRIXX for the brain field. MC = Monte Carlo

and radiation field congruence exists for the square and irregular fields studied with the MLC.

ACKNOWLEDGEMENTS

The authors wish to thank Dr. M. R. Raju, Principal Investigator of the above BRNS Project for his encouragement in carrying out this investigation. Thanks are also due to Prof. Yadagiri Reddy, Osmania University for his contributions throughout the development of the project. The authors gratefully acknowledge comments/suggestions offered during a review of the BRNS project in Jan 2013 by Dr. D. C. Kar, Dr. S. D. Sharma, Dr. Selvam, Members of the Review Committee from BRNS. Most importantly, the support of DMRL, Hyderabd in funding the prototype is acknowledged. Technical inputs from Shri M. Sankaranarayana, Senior Scientist from DMRL in the periodic reviews during fabrication of the proto MLC and constant encouragement of Dr. G. Malakondaiah, Director, DMRL are acknowledged here.

References

1. Ayyangar KM, Kumar MD, Narayan P, Jesuraj F, Raju MR. Monte Carlo simulation of a multi-leaf collimator design for telecobalt

machine using BEAMnrc code. J Med Phys 2010;35:23-32.
2. Mora GM, Maio A, Rogers DW. Monte Carlo simulation of a typical ^{60}Co therapy source. Med Phys 1999;26:2494-502.
3. Ayyangar K, Fenedict Y, Rao CR, Dinesh Kumar M, Reddy AR, Raju MR. On the design of MLC for Cobalt-60 teletherapy machine. Proceedings of 30th Annual Conference of AMPI (AMPICON-2009) Hyderabad 2009;I-26:44-5.
4. Anil Kumar T, Rajendra RS, Muralidhar KR, Ramakrishna Rao C, John MT, Ayyangar K, *et al*. Output measurements on manual multi-leaf collimator for cobalt-60 teletherapy machine. Proceedings of 31th Annual conference of AMPI [AMPICON-2010]. Lucknow 2010; O-33:8.
5. Ayyangar KM, Reddy AR, Raju MR. Development of an automated MLC for telecobalt therapy machine with a potential for conformal therapy. Proceedings of 32nd Annual conference of AMPI [AMPICON-2011] Vellore 2011; I-6:3.
6. Akula RR, Anil Kumar A, Talluri AK, Sresty M, Rao CR, Sankaranarayana M, *et al*. Calibration measurements on the prototype MLC for cobalt-60 teletherapy machine. Proceedings of 33rd Annual conference of AMPI (AMPICON- 2012); Nov 1-3, Mangalore 2012; O-06:1.
7. Anil Kumar A, Roopa Rani A, Talluri AK, Sresty M, Rao CR, Sankaranarayana M, *et al*. The use of IMatrix for the measurement of depth dose and profiles of cobalt Teletherapy machine with an automated add-on multi-leaf collimator. Proceedings of 33rd Annual conference of AMPI; AMPICON2012, Mangalore 2012. p.105-244.
8. Sahani G, Dutt Sharma S, Dash Sharma PK, Sharma DN, Hussain SA. Monte Carlo simulation based study of a proposed multileaf collimator for a telecobalt machine. Med Phys 2013;40:021705.
9. Singh IR, Ravindran BP, Ayyangar KM. Design and development of motorized multileaf collimator for telecobalt unit. Technol Cancer Res Treat 2006;5:597-605.

How to cite this article: Ayyangar KM, Rani RA, Kumar A, Reddy AR. Monte Carlo study of MLC fields for cobalt therapy machine. J Med Phys 2014;39:71-84.
Source of Support: This work is done as a part of the BRNS grant, "Development and implementation of automated multi-leaf collimator with treatment planning system as an add-on for telecobalt machine." It is a social impact project sanctioned by BRNS in April 2011.
Conflict of Interest: None declared.

Appendix A

MC simulation using full machine configuration was carried out with voxel sizes of 5 and 2.5 mm for an MLC field of 6 × 6 cm^2. The data were compared with ROPS calculation that was done with 5 mm grid spacing. When the voxel size was reduced from 5 to 2.5 mm, the voxel volume was reduced to 1/8 and computer time increased by eight times. The PDDs and profiles for x and y-directions are shown in Figure 12. Notice additional data points for 2.5 mm voxel size simulation.

From these figures of PDDs and profiles, it can be inferred that there is reasonable agreement between the results with 5 mm and 2.5 mm voxel size MC simulations; voxel size of 5 mm is adequate for most routine non-intensity-modulated radiation therapy (IMRT) conformal simulations and 2 to 2.5 mm voxel simulations for special situations of narrow fields.

Appendix B

Optical field versus radiation field

Traditionally, radiation field is compared with optical field. The optical field is generated by placing a light bulb and mirror arrangement to correspond with the source position. In the case of cobalt machine, due to the finite source size, the placement of the focal spot of the light bulb is usually made to coincide with the bottom center of the radiation source. The optical field is a pure field in the sense that the umbra is clearly the primary light photons illuminating the light field. The light edge is traditionally used as the field size set by the collimator assembly. Because the X-ray/gamma radiation is invisible, it is not possible to have such a clear edge.

The 50% radiation field width is considered as the radiation field width. Agreement between optical field and radiation field is considered as matching, if the 50% radiation field width is matching with the light field edges. Unlike the optical field that is clearly the umbra width, the radiation field edge falls in the penumbra region.

Now, let us take a look at how to find the radiation field width. It has to be measured with a scan of the whole field. The scan can be done by using a measuring device that can be a photon counter or an ionization counter such as an ionization chamber. Intensity, ionization, and dose are not equivalent. Also, many variations exist in the definitions of the maximum. When the scan is off axis, the maximum is taken as the relative maximum found on the scan ignoring the intensity at the central axis. For linear accelerator radiation beams, the maximum is complicated by the presence of horns. In cobalt, the maximum is also influenced by scattered radiation. Unlike the optical field, the radiation at the 50% levels is composed of not only primary photons but also first scattered and multiple scattered photons. The detector size and its energy response play a role in the penumbra position. Unlike the optical field width, radiation field width is dependent on two factors, the maximum intensity and the penumbra. Unfortunately, due to the reasons mentioned above there is uncertainty in the definition of the radiation field width. However, in practice due to the error allowance of 2 mm, this is not fully recognized.

When MC computations are done for cobalt, the radiation field width is even more complicated. The size of the source, the position of the collimator, the width of the collimator opening, and the height of the collimator create variations in the radiation field width.

In general, when everything else is same, the larger the size of the source, the penumbra increases and hence the optical and radiation field width congruence decreases. Similarly, the larger the collimator height, larger the collimator thickness

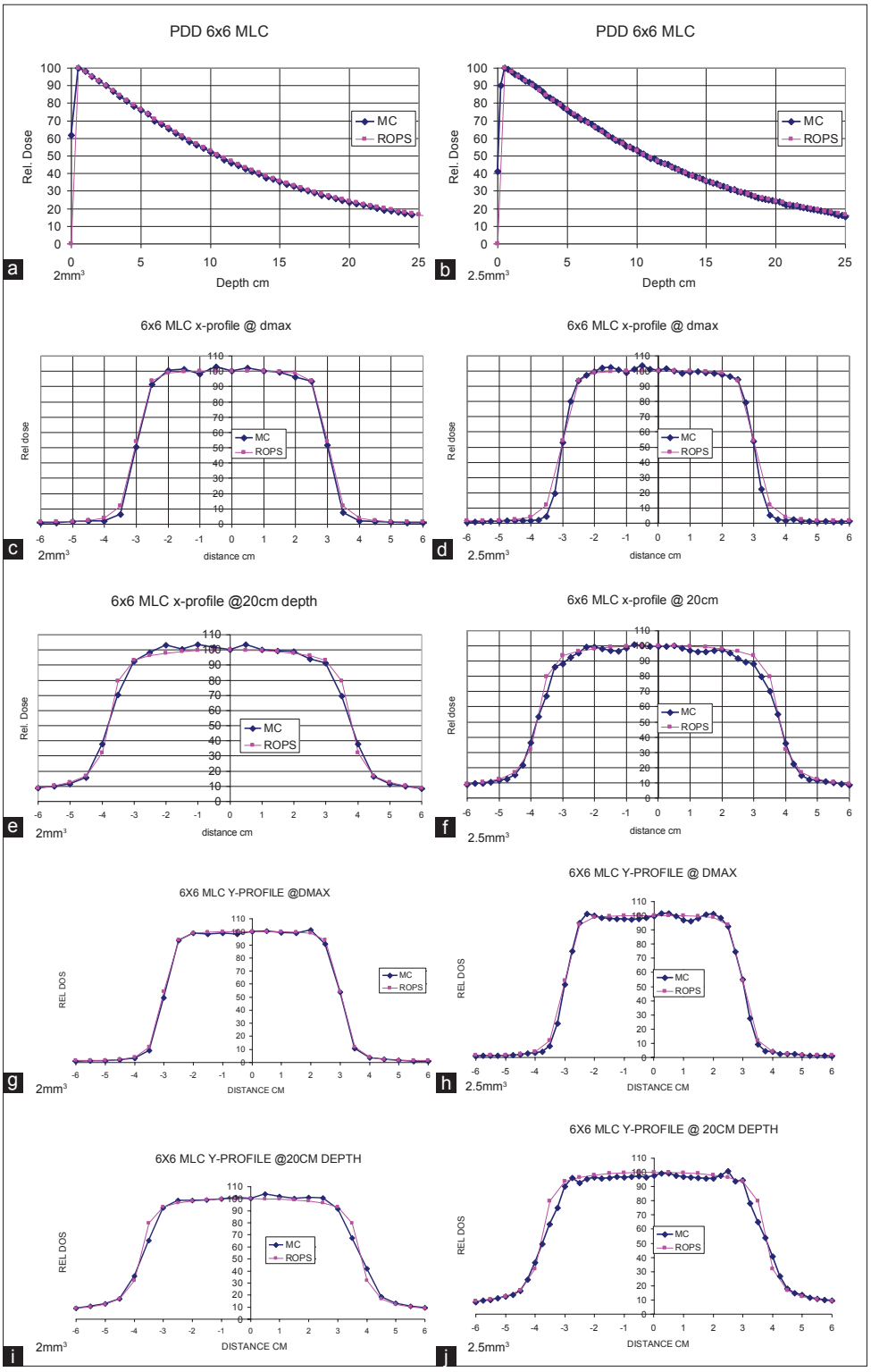

Figure 12: Results of MC simulation for a 6 × 6 cm² MLC field with 5 and 2.5 mm voxel sizes are shown in these figures. The PDD values of simulation are shown in (a) for 5 mm and in (a) for 2 mm. The profiles at dmax and at depth 20 cm for voxel size 5 mm are, respectively, shown in (c), (d) for x-direction and in (e) and (f) for y-direction. Similar profiles for 2.5 mm voxel size are shown, respectively, in (g), (h) and in (i), (j). MC = Monte Carlo, PDD = percent depth dose

and smaller the collimator opening also cause problems of the optical and radiation field width congruence.

Source and collimator

The cobalt-60 source is assumed to be a cylinder of nominal size 1.5 cm diameter and 2.0 cm height. Another assumption we made is that the source had a cladding of approximately 1 mm steel all around. Based on the measured PDD data and

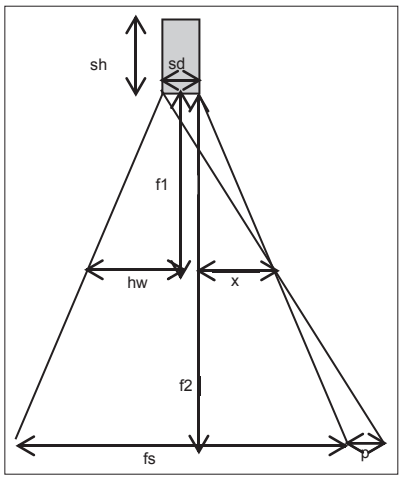

Figure 13: Schematic relationship of source size, position of telescopic collimator, penumbra, and field size at isocenter

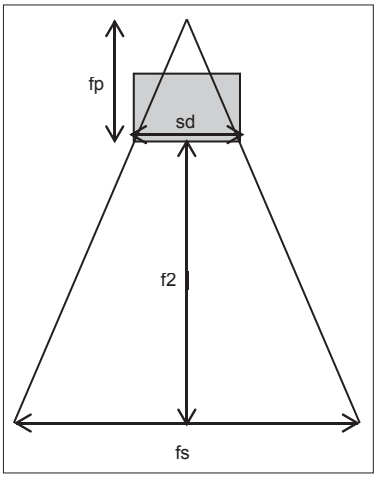

Figure 14: Geometry of the focal point of the telescopic collimator and the source and the field size at isocenter

beam profiles, these dimensions need be verified. Another parameter that need be resolved is the actual or apparent collimator geometry. The geometry description given by Mora *et al*., is depicted in Figure 2. The bottom center of the source is taken as the reference plane and origin of the coordinate system. The telescopic collimator moves in such a way that the geometric penumbra at isocenter is constant over all field sizes. To achieve this, the collimator moves with its fulcrum at the source to diaphragm distance. The geometry of this is shown in Figure 13.

The distance from the center of the source bottom to the bottom of the lower jaw is represented as *f1* and the distance to the isocenter as *f2*. If *sd* represents the source diameter, then the geometric penumbra is given by

$$p = sd*(f2 - f1)/f1$$

The field size *fs* is defined at isocenter. The value of *hw* for any arbitrary distance *f1* is determined from the relation

Table 6: Change in focal spot distance as a function of source size and field size

Focal point distance fp			
	Source diameter		
Field size	1.5	1	0.5
5×5	34.3	20	8.9
10×10	14.1	8.9	4.2
20×20	6.5	4.2	2.05

Table 7: Dependence of difference between geometric FWHM and MC-computed FWHM as a function of source diameter and field size

	Source diameter (mm)	*x-diff dmax (mm)*	*y-diff dmax (mm)*	*x-diff 20-cm depth (mm)*	*y-diff 20-cm depth (mm)*
5×5	10	1.9	1.8	2.5	2.3
5×5	15	2.2	2.5	5.3	5.1
10×10	10	1.6	1.4	1.4	1.2
10×10	15	2.1	2.4	3	3.6
20×20	10	1	1.1	−0.2	0.2
20×20	15	1.1	2.2	1.2	1.9

MC = Monte carlo, FWHM: Full width at half maximum

$$hw = f1/f2*(fs - sd)/2 + sd/2$$

The source height has no bearing on the design of the collimator.

Unlike collimators for a point source, the focal point of this collimator varies with field size and this causes complexity of the radiation properties related to the source and collimator. The Figure 14 shows the geometry of the focal point of the collimator.

The focal point distance *fp* is given by

$$fp = sd*f2/(fs - sd)$$

The change in focal spot distance from the source plane as a function of source size and field size is given in Table 6.

It can be seen that there is a large variation in the focal spot position depending on the field size. Smaller field size results in farther focal point. If the focal point is farther, one can expect the primary radiation incident on the phantom with smaller angle. This could result in relatively more intense radiation at the edges and hence larger dose to the penumbra region. This could result in slightly larger FWHM. In fact, we observed this as shown in the Table 7 above. The values are differences in calculated FWHM compared with geometric FWHM. If the source diameter is decreased, naturally the penumbra region is smaller and results in sharper beam and a smaller FWHM.